

# Phosphate-Imposed Constraints on Schwertmannite Stability under Reducing Conditions

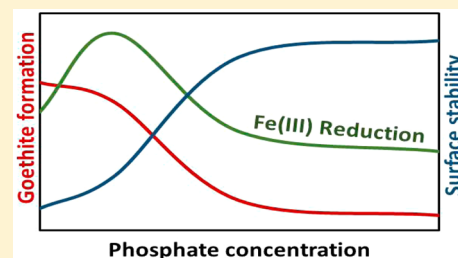
Valerie A. Schoepfer,<sup>†</sup> Edward D. Burton,<sup>\*,†</sup> Scott G. Johnston,<sup>†</sup> and Peter Kraal<sup>‡</sup>

<sup>†</sup>Southern Cross GeoScience, Southern Cross University, PO Box 157, Lismore, New South Wales 2480, Australia

<sup>‡</sup>Department of Earth Sciences—Geochemistry, Faculty of GeoSciences, Utrecht University, PO Box 80021, 3508 TA Utrecht, The Netherlands

## S Supporting Information

**ABSTRACT:** Schwertmannite is a ferric oxyhydroxysulfate mineral, which is common in acid sulfate systems. Such systems contain varying concentrations of phosphate ( $\text{PO}_4^{3-}$ )—an essential nutrient whose availability may be coupled to schwertmannite formation and fate. This study examines the effect of phosphate on schwertmannite stability under reducing conditions. Phosphate was added at 0, 80, 400, and 800  $\mu\text{moles g}^{-1}$  (i.e., zero, low, medium, and high loading) to schwertmannite suspensions which were inoculated with wetland sediment and suspended in  $\text{N}_2$ -purged artificial groundwater. pH remained between 2.7 and 4.3 over the 41 day experiment duration. Fe(II) accumulated in solution due to dissimilatory Fe(III)-reduction, which was most pronounced at intermediate  $\text{PO}_4^{3-}$  loadings (i.e., in the low  $\text{PO}_4^{3-}$  treatment). Partial transformation of schwertmannite to goethite occurred in the zero and low  $\text{PO}_4^{3-}$  treatments, with negligible transformation in higher  $\text{PO}_4^{3-}$  treatments. Overall, the results suggest that intermediate  $\text{PO}_4^{3-}$  loadings provide conditions which facilitate optimal reductive dissolution of schwertmannite. At zero  $\text{PO}_4^{3-}$  loading, reductive dissolution appears to be constrained by the rapid transformation of schwertmannite to goethite, which thereby decreases the bioavailability of solid-phase Fe(III). Conversely, at high loadings,  $\text{PO}_4^{3-}$  appears to stabilize the schwertmannite surface against dissolution; probably via the formation of strong surface complexes.



## INTRODUCTION

Acid sulfate systems are found around the world in relation to mining operations, rock weathering, and acid sulfate soils.<sup>1</sup> These systems are characterized by low pH due to the oxidation of iron sulfide minerals, such as pyrite.<sup>1</sup> One of the most common secondary minerals in acid sulfate systems is schwertmannite; a poorly crystalline iron(III) oxyhydroxysulfate.<sup>1–4</sup> Schwertmannite is metastable with regard to goethite, with previous research showing that schwertmannite is stabilized by low pH,<sup>2,3,5,6</sup> high  $\text{SO}_4^{2-}$  concentrations,<sup>3</sup> and the presence of strongly sorbed species (e.g., Si and humic/fulvic acids).<sup>6–8</sup>

The formation and stability of schwertmannite is of significant interest in acid-mine drainage (AMD) environments and in acid sulfate soils. This is because schwertmannite plays a major role in controlling water quality by influencing both the generation and consumption of acidity and by acting as a sorbent for contaminants and nutrients.<sup>9–11</sup> Although schwertmannite forms under oxidizing conditions, it may be subjected to prolonged reducing conditions in reflooded acid sulfate soils, mine pit-lake sediments or AMD-treatment wetlands.<sup>6,12</sup> Under reducing conditions, schwertmannite may strongly influence both Fe and S biogeochemistry and microbial electron flow through microbially mediated dissimilatory Fe(III)-reduction<sup>13,14</sup> or abiotic reduction by  $\text{H}_2\text{S}$  produced via dissimilatory  $\text{SO}_4^{2-}$  reduction.<sup>15</sup>

Schwertmannite is capable of sorbing large amounts of  $\text{PO}_4^{3-}$ , an essential nutrient which can also act as a pollutant depending on the levels of P in the system.<sup>16,17</sup> Collins et al.<sup>6</sup> also observed significant P-enrichment in natural schwertmannite collected from an acid sulfate soil environment. Although very little research has examined interactions between  $\text{PO}_4^{3-}$  and schwertmannite,  $\text{PO}_4^{3-}$  interactions have been extensively documented with respect to other iron(III) oxides, such as ferrihydrite, goethite and hematite.<sup>18–22</sup> Borch et al.<sup>18</sup> found that  $\text{PO}_4^{3-}$  sorption stabilizes ferrihydrite against reductive dissolution, and that it also alters secondary mineral transformation pathways. As schwertmannite and ferrihydrite are similar with respect to surface area, structural disorder, and metastability,<sup>10,23–25</sup> it can be hypothesized that schwertmannite stability may also be enhanced by the sorption of  $\text{PO}_4^{3-}$  to the mineral surface.

The objective of this study was to examine the effect of  $\text{PO}_4^{3-}$  sorption on schwertmannite stability under reducing conditions. To achieve this objective, we subjected schwertmannite, with varying loadings of added  $\text{PO}_4^{3-}$  to microbially mediated reducing conditions for 41 days and observed the aqueous and mineralogical species over time.

Received: April 24, 2017

Revised: August 2, 2017

Accepted: August 2, 2017

Published: August 2, 2017

## METHODS

**Schwertmannite Synthesis.** Schwertmannite was synthesized via the peroxide method described by Regenspurg et al.<sup>5</sup> The precipitated mineral was rinsed five times with deionized water, dried at 50 °C, and then ground to a fine powder using a ring mill.

**Phosphate Sorption Isotherm Analysis.**  $\text{PO}_4^{3-}$  sorption to schwertmannite was characterized at pH 2.6–3.0 using a batch sorption isotherm approach, involving 0.5 g of schwertmannite suspended in 40 mL of artificial groundwater (Supporting Information, SI, Table S1) with initial aqueous  $\text{PO}_4^{3-}$  concentrations of 0, 0.5, 1, 2, 3, 4, 5, 6, 6.5, 7, 7.5, 8, 9, and 10 mM, added as  $\text{KH}_2\text{PO}_4$ . After a 24-h equilibration period, the aqueous phase was separated by filtration to <0.45  $\mu\text{m}$  and retained for analysis of  $\text{PO}_4^{3-}$ .

**Reductive Incubation Experiment.** The microbial reduction experiments involved 18.75 g of synthetic schwertmannite suspended in 1.5 L of artificial groundwater (as defined above) within gastight 2 L pyrex reaction chambers. The primary carbon source for microbial processes in the reductive incubation experiment was glucose, which was present in the artificial groundwater (SI Table S1). Four replicate schwertmannite suspensions were employed for each level of  $\text{PO}_4^{3-}$  addition. Aqueous  $\text{PO}_4^{3-}$  was added to the initial artificial groundwater on the basis of the sorption isotherm results to achieve 4 differing levels of surface site coverage corresponding to 0, 80, 400, and 800  $\mu\text{mole PO}_4^{3-} \text{g}^{-1}$  schwertmannite, which are hereafter denoted as zero, low, medium, and high  $\text{PO}_4^{3-}$  treatments.

To provide a natural consortium of microorganisms, the artificial groundwater was inoculated with ~2% (w/w) benthic sediment collected from a drainage canal in the Tuckean Swamp near Lismore, Eastern Australia.<sup>26</sup> Determination of the presence and approximate numbers of iron and sulfur reducers in the initial inoculum using the most probable number (MPN) methods described by Benner et al.<sup>27</sup> and using the calculations of Garthright and Blodgett<sup>28</sup> indicated an iron reducing bacterial cell density of  $\sim 10^{7.0}$  MPN  $\text{g}^{-1}$  and a sulfur reducing bacterial cell density of  $\sim 10^{4.7}$  MPN  $\text{g}^{-1}$ .

Anoxic conditions were maintained by continuously passing high-purity  $\text{N}_{2(\text{g})}$  through the reaction chambers. The temperature was kept at 30 °C, to simulate summer temperatures, using a thermostated water-bath. The schwertmannite suspensions were manually stirred for 30 s daily over the full experimental duration of 41 days for each treatment.

At sampling times of 2, 5, 9, 13, 17, 21, 25, 29, 33, 37, and 41 days (selected on the basis of previous studies<sup>8,15,26</sup>), reaction chambers were removed from the water-bath and placed on a stir plate for 1 min to rehomogenize the suspension. A syringe was used to withdraw a 50 mL sample of homogeneous suspension, via a gastight sampling port, for characterization. The solid-phase was separated by centrifugation and dried in an anoxic chamber at room temperature (after rinsing with methanol to speed the drying process) prior to XRD analysis. The supernatant was filtered to <0.45  $\mu\text{m}$  and retained for analysis. All processing of solid- and aqueous-phase samples was conducted under strictly  $\text{O}_2$ -free conditions within an anoxic chamber.

**Analytical Methods.** The filtrate Eh and pH were measured with probes, freshly calibrated against Zobell's solution<sup>29</sup> and pH 4 and 7 buffers, respectively. One aliquot of filtrate was added to a color reagent to measure alkalinity,<sup>30</sup>

another to a 20% zinc acetate/2 M NaOH solution to preserve the sample for  $\text{H}_2\text{S}$  analysis, followed by analysis via the methylene blue method.<sup>31</sup> Samples for Fe,  $\text{SO}_4^{2-}$ , and  $\text{PO}_4^{3-}$  determination were acidified and refrigerated until analysis. Fe(II) concentrations were determined through the 1,10-phenanthroline method.<sup>32</sup> For total aqueous Fe, a sample was prereduced using hydroxylamine hydrochloride, following the same method, and Fe(III) was determined via subtraction. Phosphate was determined by the molybdenum blue method of Hansen and Koroleff in Grasshoff et al.<sup>33</sup> Sulfate was quantified by total S using a PerkinElmer Optima 8300DV Inductively Coupled Plasma Optical Emission Spectrometer (ICP-OES) after subtracting aqueous sulfide. Quantification of Fe and S content in the initial schwertmannite was performed after solid-phase digestion (1:3  $\text{HNO}_3/\text{HCl}$ ) using a PerkinElmer NexION 300D Inductively Coupled Plasma Mass Spectrometer (ICP-MS).

X-ray diffraction was used to determine the mineral phases present over time using a Phillips PW 1050/70 diffractometer with a Co X-ray tube. Samples were scanned from  $10^\circ 2\theta$  to  $80^\circ 2\theta$  using a  $0.1^\circ 2\theta$  step and a 1 s count time.

X-ray absorption spectroscopy measurements of the final (Day 41) solid-phase were made at the National Synchrotron Radiation Research Centre (NSRRC) in Hsinchu, Taiwan. Sulfur K-edge XANES data were collected under a high purity helium atmosphere on beamline 16A. Wet samples were contained between Kapton tape and Mylar film. Samples for Fe K-edge EXAFS were wet-mounted between Kapton tape and collected under normal atmosphere on beamline 17C. Standards were prepared as described by Burton and Johnston,<sup>8</sup> and were collected under identical beamline conditions to those employed for the experimental samples. To subtract the background, normalize the data, and perform linear combination fitting<sup>34</sup> (LCF), we used the ATHENA program.<sup>35</sup> No energy shifts for were allowed during the LCF. The sum of components resulting from the LCF was not forced to equal 1.

**Modeling.** Visual Minteq was used to calculate the equilibrium speciation and solubility state in solution. All species present in the initial groundwater as well as species determined analytically at each time point were included in the modeling.

## RESULTS

**Initial Schwertmannite Properties.** X-ray diffractometry confirmed that the initial mineral used in this study was schwertmannite (Figure 1a). The initial schwertmannite contained  $7.4 \pm 0.1 \text{ mmol g}^{-1}$  Fe and  $1.5 \pm 0.03 \text{ mmol g}^{-1}$  S. This Fe and S content indicate a composition of  $\text{Fe}_8\text{O}_8(\text{OH})_{4.96}(\text{SO}_4)_{1.65}$ , which is within the compositional range reported for schwertmannite.<sup>8,36,13,37</sup>

**Phosphate Sorption Isotherm Analysis.**  $\text{PO}_4^{3-}$  sorption to schwertmannite most closely followed a Freundlich isotherm, which unlike the classical Langmuir isotherm does not display a sorption capacity (Figure 2). Here, the parameter  $K_f$  is equal to  $0.63 \text{ L mmol}^{-1}$  schwertmannite with a unitless exponent ( $n$ ) of 11.6 (Figure 2). The maximum measured level of  $\text{PO}_4^{3-}$  sorption that was observed in the present study ( $\sim 650 \mu\text{moles P g}^{-1}$  schwertmannite) was comparable to Eskandarpour et al.,<sup>17</sup> who report a sorption maximum of 865  $\mu\text{moles P g}^{-1}$  schwertmannite.

**Aqueous-Phase Trends.** The pH varied as a function of time and  $\text{PO}_4^{3-}$  coverage, yet remained close to pH 3–4 (Figure 3a–d). The pH varied insignificantly with respect to

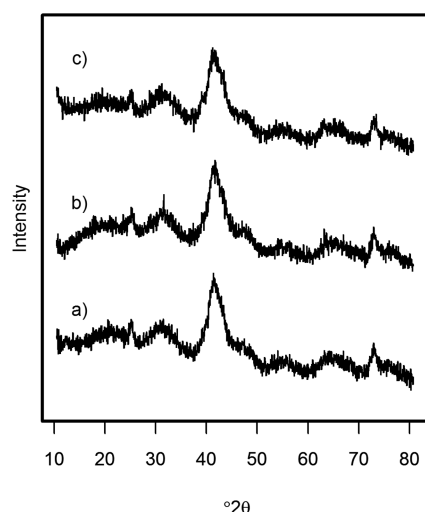


**Figure 1.** X-ray diffraction pattern for a) the initial schwertmannite, b) Day 41 medium  $\text{PO}_4^{3-}$ -treatment, and c) Day 41 high  $\text{PO}_4^{3-}$ -treatment.

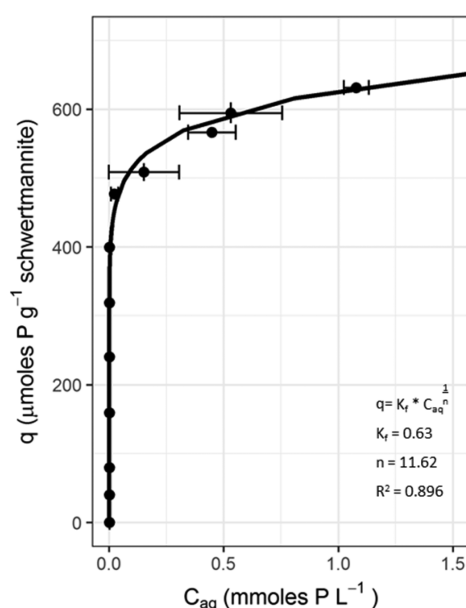


**Figure 2.** Sorption isotherm of  $\text{PO}_4^{3-}$  on schwertmannite at pH 2.6. The solid line shows the Freundlich isotherm modeled values, while the points indicate experimental values. The value  $q$  is a variable related to sorption capacity at equilibrium, while  $C_{\text{aq}}$  is the concentration of  $\text{PO}_4^{3-}$  at equilibrium. The  $R^2$  value indicates the fit of the data to the model as plotted when linearly transformed.

initial  $\text{PO}_4^{3-}$  addition (between 3.3 at zero  $\text{PO}_4^{3-}$ , and 3.0 at high  $\text{PO}_4^{3-}$ ). The highest final pH (4.3) occurred in the low  $\text{PO}_4^{3-}$  treatment, with the lowest (pH 2.7) occurring in the high  $\text{PO}_4^{3-}$  treatment.

Aqueous  $\text{PO}_4^{3-}$  concentrations were very low for the full experiment duration in the zero and low  $\text{PO}_4^{3-}$  treatments (Figure 3e,f). The medium  $\text{PO}_4^{3-}$  and high  $\text{PO}_4^{3-}$  treatments had much higher initial aqueous  $\text{PO}_4^{3-}$  concentrations (Figure 3g,h). These concentrations decreased over time, reaching steady state aqueous  $\text{PO}_4^{3-}$  concentrations of  $6.8 \mu\text{M}$  at day 5 in the medium  $\text{PO}_4^{3-}$  treatment and  $33.1 \mu\text{M}$  by day 30 in the high  $\text{PO}_4^{3-}$  treatment.

Substantial amounts of aqueous Fe(III) and Fe(II) (Figure 3i–l) developed over time in the zero, low, and medium  $\text{PO}_4^{3-}$  treatments, with very little aqueous Fe being released into solution in the high  $\text{PO}_4^{3-}$  treatment. Most aqueous Fe in all treatments existed in the 2+ oxidation state. The low  $\text{PO}_4^{3-}$  treatment had the greatest level of Fe(II) production, with an aqueous Fe(II) concentration that was close to 15 mM at day 41. There were slightly lower Fe(II) concentrations in the zero  $\text{PO}_4^{3-}$  treatment ( $\sim 10 \text{ mM}$  at day 41), and substantially less in the medium and high  $\text{PO}_4^{3-}$  treatments. Fe(II) concentrations indicate that 10%, 15%, 4.5%, and 1% of the total Fe(III) content underwent reductive dissolution in the zero, low, medium, and high  $\text{PO}_4^{3-}$  treatments, respectively (Figure 4).

Aqueous sulfide was below detection ( $< 2 \mu\text{M}$ ) in all treatments throughout the experiment. All treatments displayed an initially rapid (within 2 days) release of  $\text{SO}_4^{2-}$  into solution (Figure 3m–p). This initial release of presumably surface-bound  $\text{SO}_4^{2-}$  was dependent on the level of  $\text{PO}_4^{3-}$  addition, with higher  $\text{SO}_4^{2-}$  concentrations at day 2 (i.e., our first sample time) occurring in the higher  $\text{PO}_4^{3-}$  treatments. These aqueous concentrations correspond to rapid release of 20%, 20%, 31% and 38% of the total solid-phase  $\text{SO}_4^{2-}$  content in the zero, low, medium, and high  $\text{PO}_4^{3-}$  treatments, respectively. This is comparable to work by Bigham et al.<sup>37</sup> and Regensburg et al.<sup>13</sup> who found that  $\sim 30\%$  of  $\text{SO}_4^{2-}$  in schwertmannite is surface bound.

Following the initial rapid  $\text{SO}_4^{2-}$  release, aqueous  $\text{SO}_4^{2-}$  then increased steadily over the full experiment duration in all treatments. However, the rate of  $\text{SO}_4^{2-}$  release and hence the final extent of aqueous  $\text{SO}_4^{2-}$  production was dependent on the level of  $\text{PO}_4^{3-}$  addition. In particular, the highest final  $\text{SO}_4^{2-}$  concentrations ( $\sim 15 \text{ mM}$ ) occurred in the low  $\text{PO}_4^{3-}$  treatment, with lower concentrations occurring in the zero  $\text{PO}_4^{3-}$  treatment and even lower concentrations occurring in the medium and high  $\text{PO}_4^{3-}$  treatments. After accounting for rapid release of surface-bound  $\text{SO}_4^{2-}$  (evident at day 2), the final aqueous  $\text{SO}_4^{2-}$  concentrations equate to an additional slower release of 44%, 59%, 23%, and 21% of the total solid-phase  $\text{SO}_4^{2-}$  content (SI Figure S1).

**X-ray Diffractometry.** There was negligible change in mineralogy over 41 days in the medium and high  $\text{PO}_4^{3-}$  treatments (Figures 1b,c and S2). In contrast, XRD revealed substantial goethite formation in the zero  $\text{PO}_4^{3-}$  and low  $\text{PO}_4^{3-}$  treatments, with slightly faster transformation in the zero  $\text{PO}_4^{3-}$  treatment (Figure 5). However, both the zero and low  $\text{PO}_4^{3-}$  treatments exhibited similar XRD patterns at day 41, which reveal a mixture of crystalline goethite and poorly ordered schwertmannite.

**X-ray Absorption Spectroscopy.** The Fe K-edge EXAFS spectra for the experimental samples from day 41 are shown in Figure S3. In accordance with the XRD results, the Fe K-edge EXAFS spectra of the experimental samples were well fit by a combination of schwertmannite and goethite (Table S2). The linear combination fit (LCF) results revealed that, at day 41, the zero and low  $\text{PO}_4^{3-}$  treatments both contained close to 25% goethite, with relatively little goethite formation occurring in the medium and high  $\text{PO}_4^{3-}$  treatments (8% and 2% goethite, respectively) (Figure 6).

Sulfur K-edge XANES spectra and linear combination fitting for samples collected at day 41 are shown in SI Figure S4. These spectra show a distinct peak at  $\sim 2481 \text{ eV}$ , which corresponds to solid-phase  $\text{SO}_4^{2-}$ . The S K-edge XANES spectra also have a small peak at  $2470.6 \text{ eV}$ , which indicates the

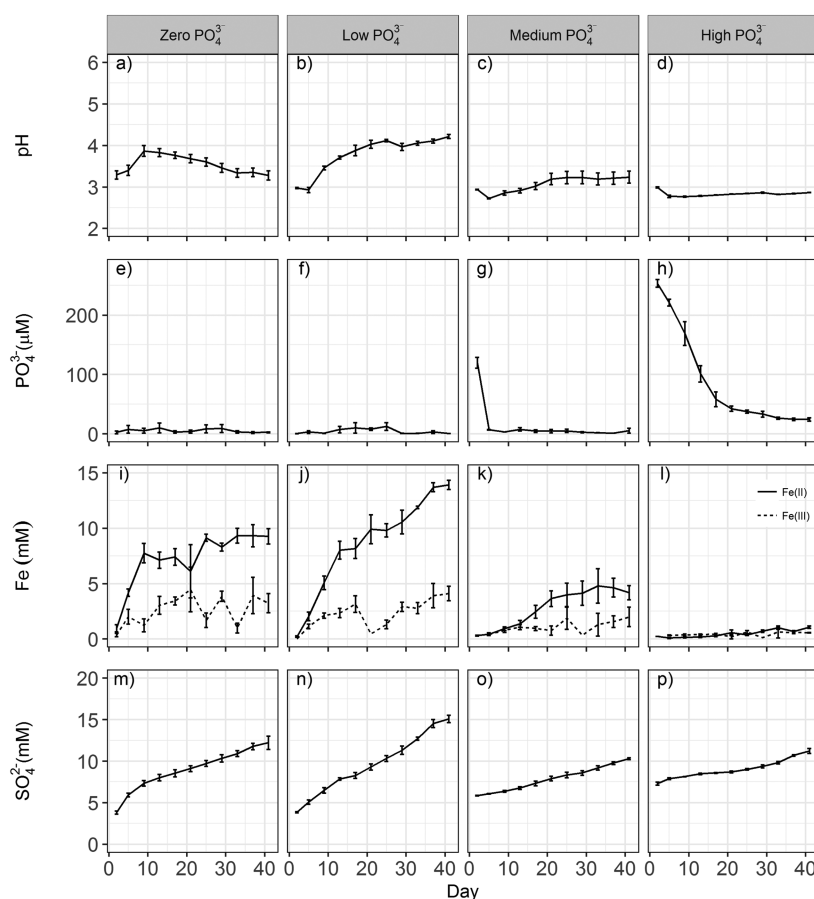


**Figure 3.** Temporal changes in pH (a–d),  $\text{PO}_4^{3-}(\text{aq})$  (e–h),  $\text{Fe}(\text{aq})$  (i–l), and  $\text{SO}_4^{2-}(\text{aq})$  (m–p) in the zero, low, medium, and high  $\text{PO}_4^{3-}$  treatments. Points are mean values of four replicates  $\pm$  standard errors.

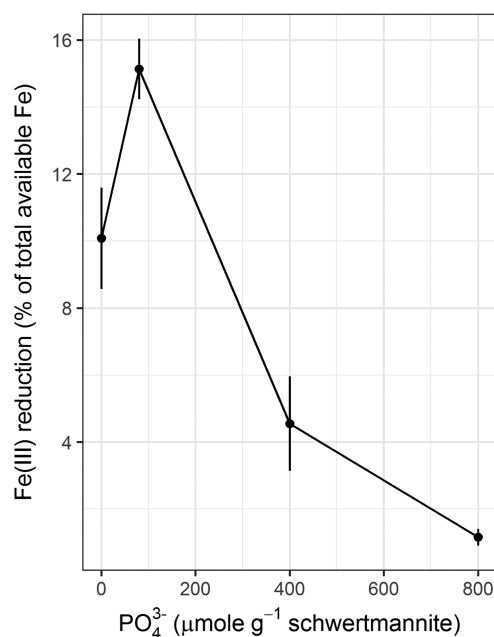


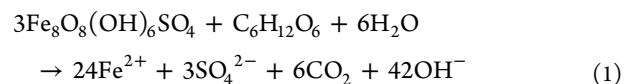
**Figure 4.** Relationship between the extent of  $\text{Fe(III)}$ -reduction and the level of  $\text{PO}_4^{3-}$  loading on the initial schwertmannite.

presence of elemental S. At day 41, 18% of the total solid-phase S in the low  $\text{PO}_4^{3-}$  sample was elemental S, whereas only 6% was elemental sulfur in the highest  $\text{PO}_4^{3-}$  treatment (Figure 6).

**Geochemical Modeling.** Geochemical modeling using Visual Minteq showed that the aqueous phase remained undersaturated with respect to vivianite throughout the experiment. However, supersaturated conditions developed with respect to strengite, a ferric phosphate mineral. It should be noted, however, that even if all  $\text{PO}_4^{3-}$  had been removed from solution via strengite formation, this would account for only about 10%, 5%, and 1% of total Fe in the high, medium and low  $\text{PO}_4^{3-}$  treatments, respectively.

## DISCUSSION

**Fe(III)-Reduction and Schwertmannite Dissolution.** The production of  $\text{Fe(II)}$  in this study can be largely attributed to the reductive dissolution of schwertmannite via the activity of dissimilatory  $\text{Fe(III)}$ -reducing microorganisms:



It should be noted that  $\text{Fe(III)}$  reduction may also involve aqueous  $\text{Fe(III)}$  to some degree, in addition to schwertmannite-bound  $\text{Fe(III)}$ .

The presence of some elemental S at day 41 suggests that  $\text{Fe(III)}$ -reduction also occurred as a result of dissimilatory  $\text{SO}_4^{2-}$  reduction (eq 2), with Peiffer and Gade<sup>38</sup> showing that abiotic reduction of schwertmannite- $\text{Fe(III)}$  by  $\text{H}_2\text{S}$  at low pH leads to the generation of  $\text{Fe(II)}$  and  $\text{S}^0$  (eq 3):



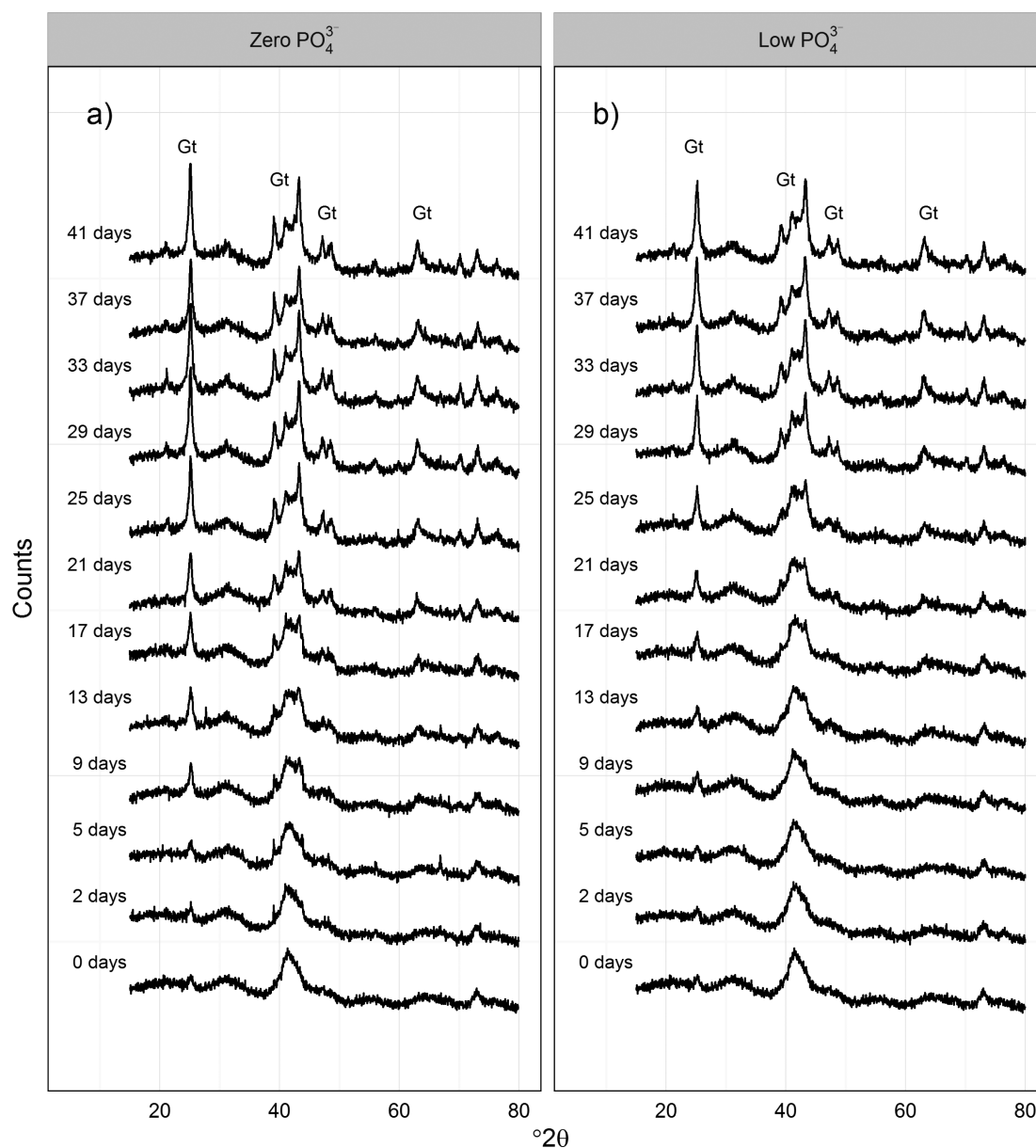
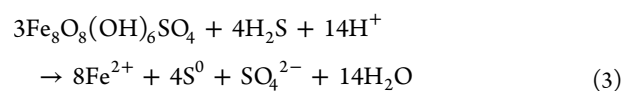
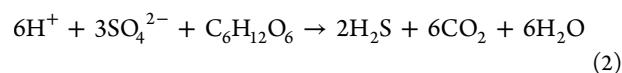


**Figure 5.** Temporal evolution of XRD patterns in the zero (a) and low (b)  $\text{PO}_4^{3-}$  treatments. The bottom pattern shows the initial schwertmannite pattern, and annotations above show goethite peaks.



Although dissimilar Fe(III)- and  $\text{SO}_4^{2-}$  reduction both produce alkalinity, the pH remained acidic for all treatments. The persistence of acidic conditions is therefore consistent with the relatively small extent of Fe(III)-reduction that occurred during the 41-day experiment. For example, the greatest degree of Fe(III) reduction (which occurred in the low  $\text{PO}_4^{3-}$  treatment) amounted to dissolution of only ~16% of the total solid-phase Fe(III). However, the mass balance between  $\text{H}^+$  production via goethite formation and  $\text{OH}^-$  production via reduction are consistent with a slowly increasing pH over the course of the 41 days (0.039, 0.066, 0.031, and 0.012 mmol  $\text{OH}^- \text{ g}^{-1} \text{ day}^{-1}$  in excess of  $\text{H}^+$  produced).

The low pH that persisted in the experiment described here is characteristic of sediment–water interfaces in acid sulfate soils and lignite mining lakes.<sup>4,13,39</sup> In these types of schwertmannite-rich systems, Fe(III) reduction is typically the dominant terminal electron accepting process.<sup>40</sup> Sulfate reduction is often assumed to require a pH of above ~4.5<sup>40</sup>, while Fe(III) reduction can occur readily at low pH.<sup>41</sup> In this experiment, the pH remained low in all treatments, and therefore, Fe(III) reduction was probably dominant. Limited sulfate reduction is also consistent with the relatively low levels of elemental S formation (which amounts to only 4.5, 4.5, 6.9, and 2.8% of the total initial S in the system as solid-phase  $\text{S}^0$ ; based on the S K-edge XAS data for the residual solid-phase S, the final aqueous  $\text{SO}_4^{2-}$  concentration and the solid/solution ratio).

**Transformation of Schwertmannite to Goethite.** In addition to releasing Fe(II), the reductive dissolution of schwertmannite also liberates  $\text{SO}_4^{2-}$  (eq 1). On the basis of

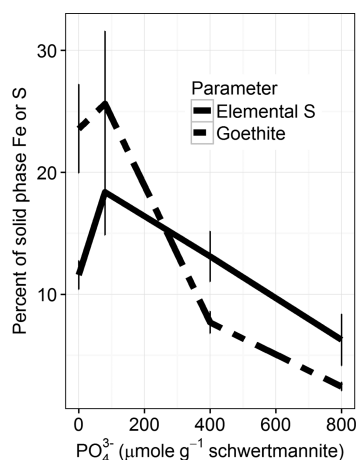
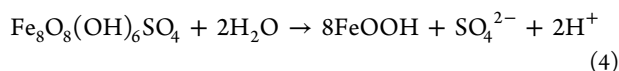


**Figure 6.** Percent elemental sulfur (solid line) and percent goethite (dashed line) expressed as a percentage of total S and total Fe, respectively, in the solid-phase at the end of the 41 day incubation in relation to the level of  $\text{PO}_4^{3-}$  loading.

the Fe(II)-derived percentages of reductive dissolution mentioned above, the corresponding aqueous  $\text{SO}_4^{2-}$  concentrations (based on congruent dissolution) would be expected to be no greater than 1.9, 2.9, 0.9, and 0.2 mM for the zero, low, medium, and high  $\text{PO}_4^{3-}$  treatments, respectively. However, these expected concentrations of  $\text{SO}_4^{2-}$  equate to only between 2% and 19% of the actual aqueous  $\text{SO}_4^{2-}$  concentrations that developed over the duration of this experiment.

This discrepancy reflects the presence of an additional  $\text{SO}_4^{2-}$  source, which can be largely explained by the mineralogical transformation of schwertmannite to goethite and subsequent release of structural  $\text{SO}_4^{2-}$  (eq 4):



XRD showed clear evidence of goethite formation in the two lowest  $\text{PO}_4^{3-}$  treatments (Figure 5a,b), which was corroborated by the Fe K-edge EXAFS spectroscopy results. Goethite transformation was fastest in the zero  $\text{PO}_4^{3-}$  treatment due to the lack of sorbing ions.<sup>8,15,26,42</sup> The Fe EXAFS data also indicate some minor schwertmannite transformation in the two higher  $\text{PO}_4^{3-}$  treatments. This concurs with the small increase in aqueous  $\text{SO}_4^{2-}$  that occurred in the medium and high  $\text{PO}_4^{3-}$  treatments between day 2 and 41.

The Fe K-edge EXAFS data indicate that ~25% of the initial schwertmannite transformed to goethite over the 41 day experiment in the low  $\text{PO}_4^{3-}$  treatment, with slightly less transformation occurring in the zero  $\text{PO}_4^{3-}$  treatment. This extent of schwertmannite transformation is comparable to that observed by Knorr and Blodau,<sup>43</sup> who found between 25% and 34% transformation in the absence of  $\text{PO}_4^{3-}$  over 100 days at pH 3 and 20 °C.

Burton et al.<sup>42,15,8,26</sup> have previously documented much faster rates of schwertmannite transformation under Fe(III) reducing conditions than those observed in the zero  $\text{PO}_4^{3-}$  treatment. For example, Burton et al.<sup>42</sup> found complete transformation of schwertmannite to goethite over just a few hours at near-neutral pH as a result of an abiotic Fe(II)-catalyzed transformation pathway. Burton and Johnston<sup>8</sup> found that, in the absence of elevated  $\text{PO}_4^{3-}$  concentrations, ~60% to ~80% of schwertmannite-derived Fe(III) was microbially reduced to Fe(II) within 20 days, causing pH to increase

from pH ~3.5 to ~6.5 and thereby triggering almost complete transformation of schwertmannite to goethite. The present work differs from these earlier studies in that the earlier microbially mediated experiments quickly developed near-neutral pH, which is required for the surface complexation of  $\text{Fe}^{2+}$  that ultimately drives rapid  $\text{Fe}^{2+}$ -catalyzed transformation of schwertmannite to goethite.

Relatively slow initiation of Fe(III) reduction in the present study was possibly influenced by the absence of additional humic acid in the artificial groundwater, while glucose acted as the primary electron donor for microbial activity. Humic acid can act as an electron shuttle in microbial Fe(III) reduction.<sup>44–46</sup> Consequently, it is hypothesized that without humic acid, as in this study, Fe(III) reduction may have been slowed, thereby inhibiting alkalinity production via Fe(III) reduction and helping to retain acidic conditions.

#### Phosphate Imposed Constraints: An Optimal Zone.

Our study shows a nonlinear response of schwertmannite reduction to  $\text{PO}_4^{3-}$  surface coverage over a 41-day period. Indicators of microbially mediated reduction of Fe(III) in this study include the formation of both Fe(II) and elemental S. Both reaction products display a similar and distinct optimal range with respect to  $\text{PO}_4^{3-}$  coverage on schwertmannite (Figure 4 and SI Figure S1). More specifically, conditions for schwertmannite reduction are optimal at partial coverage by  $\text{PO}_4^{3-}$ . Previous research has documented inhibition of ferrihydrite reduction with increasing levels of  $\text{PO}_4^{3-}$  addition.<sup>18</sup> The current study expands on this prior work examining ferrihydrite by demonstrating a more complex, nonlinear effect on schwertmannite stability in response to  $\text{PO}_4^{3-}$  loading.

Small amounts of  $\text{PO}_4^{3-}$  are known to enhance Fe(III) reduction in Fe(III) oxide species under near-neutral conditions,<sup>47–49</sup> which is consistent with the elevated reduction of schwertmannite in the low  $\text{PO}_4^{3-}$  treatment (although caution must be taken when extrapolating to the acidic conditions of the present experiment). These previous studies suggest that Fe–P compounds may enhance reduction by scavenging Fe(II) from the mineral surface. While  $\text{PO}_4^{3-}$  is an essential nutrient which may possibly promote greater levels of microbial activity at higher loadings, such nutrient-driven enhancement of Fe(III)-reduction cannot explain the observed maxima in schwertmannite reduction at intermediate  $\text{PO}_4^{3-}$  loadings. Rather, other mechanisms relating to mineral stabilization and transformation overshadow the potential nutrient enhancement in this system.  $\text{PO}_4^{3-}$  has been found to have an inhibitory effect on Fe(III) oxide reduction. This inhibition has previously been shown with  $\text{PO}_4^{3-}$  sorption to ferrihydrite.<sup>18,50–52</sup>  $\text{PO}_4^{3-}$  can bind to Fe(III) oxides by exchanging two hydroxyl groups and bridging the corners of the mineral polyhedra.<sup>53,54</sup> Dissolution and reduction are inhibited due to the high activation energy required to break this Fe(III)–O–P bond.<sup>53</sup> Therefore, this may be an important mechanism attenuating Fe(III) reduction at higher  $\text{PO}_4^{3-}$  sorption levels.

**Environmental Implications.** This study demonstrates that  $\text{PO}_4^{3-}$  can act to enhance schwertmannite–Fe(III) reduction at intermediate  $\text{PO}_4^{3-}$  loadings, and act as a barrier to schwertmannite–Fe(III) reduction at high  $\text{PO}_4^{3-}$  loadings. At zero  $\text{PO}_4^{3-}$  coverage, rapid transformation to goethite appears to partially inhibit dissimilatory Fe(III) reduction. As the level of  $\text{PO}_4^{3-}$  loading increases, there is an optimal zone of  $\text{PO}_4^{3-}$  coverage at which reduction of Fe(III) is enhanced. The

$\text{PO}_4^{3-}$  loadings used here were selected to be environmentally relevant for acid sulfate systems, as many of these environments may receive significant agricultural input or experience dynamic redox characteristics and therefore localized  $\text{PO}_4^{3-}$  hotspots. Small amounts of  $\text{PO}_4^{3-}$  ( $\sim 45 \mu\text{moles P g}^{-1}$  schwertmannite) have been previously documented in schwertmannite-rich environments<sup>6</sup> and the results of this study may help in understanding the persistence of schwertmannite under these and higher  $\text{PO}_4$  loadings. This study provides new insight into how interactions between  $\text{PO}_4^{3-}$  and schwertmannite may affect Fe(III) reduction and Fe mineral evolution at low pH.

## ■ ASSOCIATED CONTENT

### Supporting Information

The Supporting Information is available free of charge on the ACS Publications website at DOI: 10.1021/acs.est.7b02103.

Slow release sulfur data, medium and high phosphate treatment XRD patterns, iron and sulfur XAS fits and linear combination fitting parameters (PDF)

## ■ AUTHOR INFORMATION

### Corresponding Author

\*E-mail: ed.burton@scu.edu.au (E.D.B.).

### ORCID

Valerie A. Schoepfer: 0000-0002-9582-9940

Edward D. Burton: 0000-0002-9628-089X

Scott G. Johnston: 0000-0002-5826-5613

### Author Contributions

The manuscript was written through the contributions of all authors. All authors have approved the final version of the manuscript.

### Notes

The authors declare no competing financial interest.

## ■ ACKNOWLEDGMENTS

Funding was provided by the Australian Research Council (grant LP LP120200723). We also thank the NSRRC in Taiwan for facilitating the collection of XAS data. P.K. further wishes to acknowledge NWO Veni grant 863.14.014.

## ■ REFERENCES

- (1) Bigham, J. M.; Nordstrom, D. K. Iron and aluminum hydroxysulfates from acid sulfate waters. *Rev. Mineral. Geochem.* **2000**, *40* (1), 351–403.
- (2) Bigham, J.; Schwertmann, U.; Traina, S.; Winland, R.; Wolf, M. Schwertmannite and the chemical modeling of iron in acid sulfate waters. *Geochim. Cosmochim. Acta* **1996**, *60* (12), 2111–2121.
- (3) Jönsson, J.; Persson, P.; Sjöberg, S.; Lövgren, L. Schwertmannite precipitated from acid mine drainage: phase transformation, sulphate release and surface properties. *Appl. Geochem.* **2005**, *20*, 179–191.
- (4) Blodau, C. Evidence for a hydrologically controlled iron cycle in acid and iron rich sediments. *Aquat. Sci.* **2004**, *66* (1), 47–59.
- (5) Regenspurg, S.; Brand, A.; Peiffer, S. Formation and stability of schwertmannite in acidic mining lakes. *Geochim. Cosmochim. Acta* **2004**, *68* (6), 1185–1197.
- (6) Collins, R. N.; Jones, A. M.; Waite, T. D. Schwertmannite stability in acidified coastal environments. *Geochim. Cosmochim. Acta* **2010**, *74* (2), 482–496.
- (7) Jones, A. M.; Collins, R. N.; Rose, J.; Waite, T. D. The effect of silica and natural organic matter on the Fe(II)-catalysed transformation and reactivity of Fe(III) minerals. *Geochim. Cosmochim. Acta* **2009**, *73* (15), 4409–4422.
- (8) Burton, E. D.; Johnston, S. G. Impact of silica on the reductive transformation of schwertmannite and the mobilization of arsenic. *Geochim. Cosmochim. Acta* **2012**, *96*, 134–153.
- (9) Fukushi, K.; Sasaki, M.; Sato, T.; Yanase, N.; Amano, H.; Ikeda, H. A natural attenuation of arsenic in drainage from an abandoned arsenic mine dump. *Appl. Geochem.* **2003**, *18* (8), 1267–1278.
- (10) Regenspurg, S.; Peiffer, S. Arsenate and chromate incorporation in schwertmannite. *Appl. Geochem.* **2005**, *20*, 1226–1239.
- (11) Antelo, J.; Fiol, S.; Gondar, D.; Pérez, C.; López, R.; Arce, F. Cu(II) incorporation to schwertmannite: Effect on stability and reactivity under AMD conditions. *Geochim. Cosmochim. Acta* **2013**, *119*, 149–163.
- (12) Küsel, K.; Dorsch, T.; Acker, G. Microbial Reduction of Fe(III) in Acidic Sediments: Isolation of Acidiphilium cryptum JF-5 Capable of Coupling the Reduction of Fe(III) to the Oxidation of Glucose. *Appl. Environ. Microbiol.* **1999**, *65* (8), 3633–3640.
- (13) Regenspurg, S.; Goßner, A.; Peiffer, S.; Kusel, K. Potential remobilization of toxic anions during reduction of arsenated and chromated schwertmannite by the dissimilatory Fe(III)-Reducing bacterium Acidiphilium cryptum JF-5. *Water, Air, Soil Pollut.: Focus* **2002**, *2*, 57–67.
- (14) Küsel, K.; Dorsch, T. Effect of supplemental electron donors on the microbial reduction of Fe(III), sulfate, and CO<sub>2</sub> in mining-impacted freshwater lake sediments. *Microb. Ecol.* **2000**, *40*, 238–249.
- (15) Burton, E. D.; Bush, R. T.; Sullivan, L. A.; Mitchell, D. R. G. Reductive transformation of iron and sulfur in schwertmannite-rich accumulations associated with acidified coastal lowlands. *Geochim. Cosmochim. Acta* **2007**, *71*, 4456–4473.
- (16) Boers, P. C. M.; Van Raaphorst, W.; Van Der Molen, D. T. Phosphorus retention in sediments. *Water Sci. Technol.* **1998**, *37* (3), 31–39.
- (17) Eskandarpour, A.; Sassa, K.; Bando, Y.; Okido, M.; Asai, S. Magnetic Removal of Phosphate from Wastewater Using Schwertmannite. *Mater. Trans.* **2006**, *47* (7), 1832–1837.
- (18) Borch, T.; Masue, Y.; Kukkadapu, R. K.; Fendorf, S. Phosphate imposed limitations on biological reduction and alteration of ferrihydrite. *Environ. Sci. Technol.* **2007**, *41*, 166–172.
- (19) Latta, D. E.; Bachman, J. E.; Scherer, M. M. Fe electron transfer and atom exchange in goethite: Influence of Al-substitution and anion sorption. *Environ. Sci. Technol.* **2012**, *46* (19), 10614–10623.
- (20) Hinkle, M. A. G.; Catalano, J. G. Effect of phosphate and sulfate on Ni repartitioning during Fe(II)-catalyzed Fe(III) oxide mineral recrystallization. *Geochim. Cosmochim. Acta* **2015**, *165*, 62–74.
- (21) Voegelin, A.; Senn, A. C.; Kaegi, R.; Hug, S. J.; Mangold, S. Dynamic Fe-precipitate formation induced by Fe(II) oxidation in aerated phosphate-containing water. *Geochim. Cosmochim. Acta* **2013**, *117*, 216–231.
- (22) Biber, M. V.; dos Santos Afonso, M.; Stumm, W. The coordination chemistry of weathering: IV. Inhibition of the dissolution of oxide minerals. *Geochim. Cosmochim. Acta* **1994**, *58* (9), 1999–2010.
- (23) Antelo, J.; Fiol, S.; Gondar, D.; López, R.; Arce, F. Comparison of arsenate, chromate and molybdate binding on schwertmannite: surface adsorption vs anion-exchange. *J. Colloid Interface Sci.* **2012**, *386* (1), 338–343.
- (24) Enyard, A. Relationship of well and poorly crystallized iron oxides with phosphate and water retention by soils: a review. *Miner. Petrogr. Acta* **1993**, *36*, 343–350.
- (25) Paikaray, S.; Göttlicher, J.; Peiffer, S. Removal of As(III) from acidic waters using schwertmannite: Surface speciation and effect of synthesis pathway. *Chem. Geol.* **2011**, *283* (3–4), 134–142.
- (26) Burton, E.; Johnston, S.; Kraal, P.; Bush, R. T.; Claff, S. R. Sulfate availability drives divergent evolution of arsenic speciation during microbially mediated reductive transformation of schwertmannite. *Environ. Sci. Technol.* **2013**, *47*, 2221–2229.
- (27) Benner, S. G.; Gould, W. D.; Blowes, D. W. Microbial populations associated with the generation and treatment of acid mine drainage. *Chem. Geol.* **2000**, *169* (3–4), 435–448.

- (28) Garthright, W. E.; Blodgett, R. J. FDA's preferred MPN methods for standard, large or unusual tests, with a spreadsheet. *Food Microbiol.* **2003**, *20* (4), 439–445.
- (29) Zobell, C. E. Studies on redox potentials of marine sediments. *Bull. Am. Assoc. Pet. Geol.* **1946**, *30*, 477–513.
- (30) Sarazin, G.; Michard, G.; Prevot, F. A rapid and accurate spectroscopic method for alkalinity measurements in sea water samples. *Water Res.* **1999**, *33* (1), 290–294.
- (31) Cline, J. Spectrophotometric determination of hydrogen sulfide in natural waters. *Limnol. Oceanogr.* **1969**, *14*, 454–458.
- (32) APHA. Standard methods for the examination of water and wastewater. *Health Laboratory Science* 2005; pp 137–141.
- (33) Grasshoff, K.; Kremling, K.; Ehrhardt, M. *Methods of Seawater Analysis*, 3<sup>rd</sup> ed.; New York, 1999; Vol. 7.
- (34) Burton, E. D.; Bush, R. T.; Johnston, S. G.; Watling, K. M.; Hocking, R. K.; Sullivan, L. A.; Parker, G. K. Sorption of arsenic(V) and arsenic(III) to schwertmannite. *Environ. Sci. Technol.* **2009**, *43* (24), 9202–9207.
- (35) Ravel, B.; Newville, M. ATHENA, ARTEMIS, HEPHAESTUS: Data analysis for X-ray absorption spectroscopy using IFEFFIT. *J. Synchrotron Radiat.* **2005**, *12* (4), 537–541.
- (36) Burton, E. D.; Johnston, S. G.; Watling, K.; Bush, R. T.; Keene, A. F.; Sullivan, L. A. Arsenic effects and behavior in association with the Fe(II)-catalyzed transformation of schwertmannite. *Environ. Sci. Technol.* **2010**, *44* (6), 2016–2021.
- (37) Acero, P.; Ayora, C.; Torrentó, C.; Nieto, J.-M. The behavior of trace elements during schwertmannite precipitation and subsequent transformation into goethite and jarosite. *Geochim. Cosmochim. Acta* **2006**, *70*, 4130–4139.
- (38) Peiffer, S.; Gade, W. Reactivity of ferric oxides toward H<sub>2</sub>S at low pH. *Environ. Sci. Technol.* **2007**, *41* (9), 3159–3164.
- (39) Blodau, C. A review of acidity generation and consumption in acidic coal mine lakes and their watersheds. *Sci. Total Environ.* **2006**, *369* (1–3), 307–332.
- (40) Peine, A.; Tritschler, A.; Küsel, K.; Peiffer, S. Electron flow in an iron-rich acidic sediment: evidence for an acidity-driven iron cycle. *Limnol. Oceanogr.* **2000**, *45* (5), 1077–1087.
- (41) Küsel, K.; Dorsch, T.; Acker, G. Microbial Reduction of Fe (III) in Acidic Sediments: Isolation of *Acidiphilium cryptum* JF-5 Capable of Coupling the Reduction of Fe (III) to the Oxidation of Glucose Microbial Reduction of Fe (III) in Acidic Sediments: Isolation of *Acidiphilium* cr. *Appl. Environ. Microbiol.* **1999**, *65* (8), 3633–3640.
- (42) Burton, E. D.; Bush, R. T.; Sullivan, L. a.; Mitchell, D. R. G. Schwertmannite transformation to goethite via the Fe(II) pathway: Reaction rates and implications for iron–sulfide formation. *Geochim. Cosmochim. Acta* **2008**, *72*, 4551–4564.
- (43) Knorr, K.-H.; Blodau, C. Controls on schwertmannite transformation rates and products. *Appl. Geochem.* **2007**, *22* (9), 2006–2015.
- (44) Nevin, K.; Lovley, D. Potential for Nonenzymatic Reduction of Fe(III) via Electron Shuttling in Subsurface Sediments. *Environ. Sci. Technol.* **2000**, *34*, 2472–2478.
- (45) Kappler, A.; Benz, M.; Schink, B.; Brune, A. Electron shuttling via humic acids in microbial iron(III) reduction in a freshwater sediment. *FEMS Microbiol. Ecol.* **2004**, *47* (1), 85–92.
- (46) Amstatter, K.; Borch, T.; Kappler, A. Influence of humic acid imposed changes of ferrihydrite aggregation on microbial Fe(III) reduction. *Geochim. Cosmochim. Acta* **2012**, *85* (May), 326–341.
- (47) Kukkadapu, R. K.; Zachara, J. M.; Fredrickson, J. K.; Kennedy, D. W. Biotransformation of two-line silica-ferrihydrite by a dissimilatory Fe(III)-reducing bacterium: Formation of carbonate green rust in the presence of phosphate. *Geochim. Cosmochim. Acta* **2004**, *68* (13), 2799–2814.
- (48) Zachara, J. M.; Fredrickson, J. K.; Smith, S.; Gassman, P. L. Solubilization of Fe (III) oxide-bound trace metals by a dissimilatory Fe (III) reducing bacterium. *Geochim. Cosmochim. Acta* **2001**, *65* (1), 75–93.
- (49) Fredrickson, J. K.; Zachara, J. M.; Kennedy, D. W.; Dong, H.; Onstott, T. C.; Hinman, N. W.; Li, S. M. Biogenic iron mineralization accompanying the dissimilatory reduction of hydrous ferric oxide by a groundwater bacterium. *Geochim. Cosmochim. Acta* **1998**, *62* (19–20), 3239–3257.
- (50) Willett, I. R. The Reductive Dissolution of Phosphated Ferrihydrite and Strengite. *Aust. J. Soil Res.* **1985**, *23*, 237–244.
- (51) Galvez, N.; Barron, V.; Torrent, J. Effect of phosphate on the crystallization of hematite, goethite, and lepidocrocite from ferrihydrite. *Clays Clay Miner.* **1999**, *47* (3), 304–311.
- (52) Borch, T.; Fendorf, S. Chapter 12 Phosphate Interactions with Iron (Hydr)oxides: Mineralization Pathways and Phosphorus Retention upon Bioreduction. *Dev. Earth Environ. Sci.* **2007**, *7*, 321–348.
- (53) Stumm, W. Reactivity at the mineral-water interface: Dissolution and inhibition. *Colloids Surf., A* **1997**, *120* (1–3), 143–166.
- (54) Bondietti, G.; Sinniger, J.; Stumm, W. The reactivity of Fe(III) (hydr)oxides: effects of ligands in inhibiting the dissolution. *Colloids Surf., A* **1993**, *79*, 157–167.